

Bromination of Graphene and Graphite

A. Yaya¹, C. P. Ewels^{1,*}, I. Suarez-Martinez^{1,2}, Ph. Wagner¹,
S. Lefrant¹, A. Okotrub³, L. Bulusheva³, and P. R. Briddon⁴

¹ *Institut des Matériaux Jean Rouxel, Université de Nantes, CNRS UMR 6502, 44322 Nantes, France*

² *Nanochemistry Research Institute, Curtin University of Technology, Perth, WA 6845, Australia*

³ *Nikolaev Institute of Inorganic Chemistry SB RAS, 3 Acad. Lavrentiev avenue, Russia and*

⁴ *School of Natural Sciences, University of Newcastle upon Tyne, Newcastle upon Tyne, UK*

(Dated: August 17, 2021)

For full reference please see: Phys. Rev. B 83, 045411, 2011

We present a density functional theory study of low density bromination of graphene and graphite, finding significantly different behaviour in these two materials. On graphene we find a new Br₂ form where the molecule sits perpendicular to the graphene sheet with an extremely strong molecular dipole. The resultant Br⁺-Br⁻ has an empty p_z-orbital located in the graphene electronic π -cloud. Bromination opens a small (86meV) band gap and strongly dopes the graphene. In contrast, in graphite we find Br₂ is most stable parallel to the carbon layers with a slightly weaker associated charge transfer and no molecular dipole. We identify a minimum stable Br₂ concentration in graphite, finding low density bromination to be endothermic. Graphene may be a useful substrate for stabilising normally unstable transient molecular states.

PACS numbers: 31.15.A- 73.22.Pr 81.05.uf 37.30.+i

The intercalation of carbon nanomaterials with electron donors and acceptors is an active research area in which much effort is channelled towards the understanding and controlling of the electronic properties of graphene and graphite. Numerous potential applications such as sensors, electronic display panels, hydrogen storage and supercapacitors¹ have been suggested for such intercalated materials. The layered structure of graphites plays an important role in charge transfer reactions. Acceptor species can intercalate between graphitic layers, expanding the graphite with the resultant hybrids known as graphite intercalated compounds².

Bromine acts as an acceptor when intercalated in materials such as graphite or nanotubes, and has been proposed experimentally as a way to open a band gap in 3- or 4- layer graphene³. The in- plane electrical conductivity of graphite increases from $2.4 \times 10^4 \Omega^{-1}\text{cm}^{-1}$ at room temperature to $2.2 \times 10^5 \Omega^{-1}\text{cm}^{-1}$ after intercalation with bromine².

Bromine forms many ordered phases in graphites and undergoes an order-disorder phase transition as the amount of bromine or temperature changes^{2,4-8}. Bromine intercalated graphite forms stage- n compounds where n is the number of graphitic layers between planes of Br₂ ($n > 1$ ⁹). Extended X-ray Absorption Fine Structure (EXAFS) spectroscopy at room temperature and 100K¹⁰ showed that intercalated bromine molecules lie parallel to the basal plane, with an expansion of the Br-Br distance by 0.03 Å to accommodate the lattice mismatch between the free molecule and the 2.46 Å spacing between graphite hexagons. X-ray diffraction and electron microscopy studies⁶ suggest that intercalated Br₂ at lower concentration is composed of chains of Br₂ molecules in which the intermolecular distances is identical to that of solid bromine.

Graphite Raman spectra associated with Br₂ intercalation show a strong peak at 242 cm^{-1} ¹¹⁻¹⁴ assigned to the intercalated Br₂ stretch mode. The frequency is downshifted from 320 cm^{-1} for gaseous Br₂ and 295 cm^{-1} for solid molecular bromine¹⁵. There have been limited density functional studies of brominated graphite¹⁶ and graphene^{1,17}.

In this paper we examine low density bromination of graphene and graphite using density functional (DFT) calculations within the local density approximation¹⁸. The method has been successfully used to study intercalated boron in graphite¹⁹. A localised Gaussian basis set is used with a large number of fitting functions per atom (22 for each C atom and 50 for each Br), with angular momenta up to $l=2$ for C and $l=3$ for Br. A finite temperature electron level filling of $kT=0.04\text{eV}$ is used to improve convergence. Core electrons were eliminated using norm-conserving relativistic pseudopotentials of Hartwigsen, Goedecker and Hutter²⁰. A cut-off energy of 150 Hartrees was used to obtain convergence of the charge density.

Isolated Br₂ was calculated in a 13.23 \AA cubic supercell. Hexagonal 4×4 graphene supercells containing C₃₂Br₂ were used with a large vacuum spacing of 31 \AA between layers to ensure no inter- layer interaction, and a $4 \times 4 \times 1$ Monkhorst-Pack k-point grid²¹. Graphite calculations used $3 \times 3 \times n$ layer supercells (C₁₈) _{n} (Br₂) _{m} , $n=1-4$, $m=1-2$) for different layer stackings, with $4 \times 4 \times 1$ or $4 \times 4 \times 2$ k-point grids depending on cell size. All structures were fully geometrically optimised with no constraints of symmetry, allowing both atomic positions and cell dimensions to vary freely. Atomic charge states were obtained by summing Mulliken population analysis over all the filled electronic states. Vibrational frequencies were calculated by determining the energy and forces

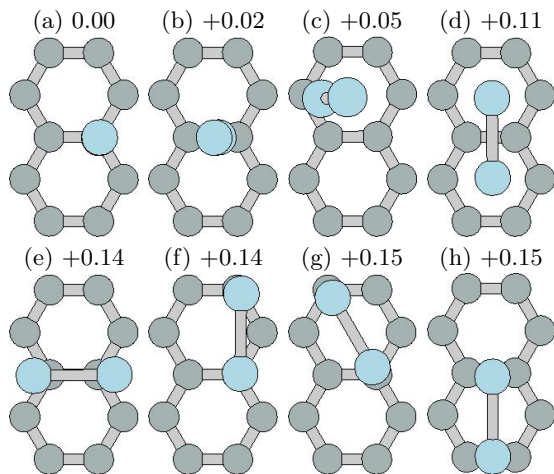


FIG. 1. Optimised geometries of Br_2 molecule perpendicular (a-c) and parallel (d-h) to a graphene sheet. Relative stabilities are quoted in eV (binding energy of Br_2 in structure (a) is 0.40eV). The text refers to (a) Br_2^\perp and (d) Br_2^\parallel

TABLE I. Calculated parameters for the most stable Br_2^\perp and Br_2^\parallel on graphene compared with literature DFT calculations.

	Br_2^\perp	Br_2^\parallel	Literature
Orientation	Perp.	Parallel	Parallel
Binding energy / Br_2 (eV)	-0.40	-0.29	-0.20 ¹ -0.29 ¹⁷
Br-Br Stretch Frequency (cm^{-1})	288	270	311 ¹
Br-Br bond length (\AA)	2.33	2.31	2.245 ¹
Br-C distance (\AA)	2.74	3.45	3.375 ¹ 3.74 ¹⁷
Charge state of Br atoms (e)	+0.48	-0.04	
	-0.61	-0.04	
Total Charge transfer / Br_2 (e)	-0.13	-0.08	

for ± 0.2 au displacements of the Bromine atoms. The second derivatives on the displaced atoms can then be found from the two-sided difference formula for the second derivative. All results are spin averaged, test calculations with spin polarisation all gave zero spin solutions as the most thermodynamically stable.

Our calculated bond length, 2.29 \AA , and stretching frequency, 326 cm^{-1} , for isolated Br_2 show excellent agreement with experiment (2.27 \AA and 323 cm^{-111} , 2.283 \AA and 320 cm^{-113}) and literature DFT/LDA values (2.263 \AA^{22} , 2.244 \AA and 324 cm^{-11}).

Figure 1 shows the structures of Br_2 over graphene in both perpendicular and parallel orientations after geometry optimisation, with calculated properties for Br_2^\perp and Br_2^\parallel (structures (a) and (d) respectively in Figure 1) in Table I.

The most thermodynamically stable arrangement is Br_2 oriented perpendicular to the graphene sheet above a carbon atom (Figure 1a, referred to hereafter as Br_2^\perp

). Its binding energy of 0.40eV shows it will be strongly physisorbed at room temperature. However the small variations in binding energy between structures suggests that low density Br_2 binding to graphene will be largely orientation independent; indeed and at these densities at room temperature Br_2 should be in constant tumbling motion (this also holds for the results of¹⁷). Increasing Br_2 concentration did not significantly change the relative energies of perpendicular and parallel orientations. However it is possible to obtain twice the maximum surface density for Br_2^\perp as for Br_2 in the parallel orientation (Figure 1d, referred to hereafter as Br_2^\parallel). Thus for the limit of high surface concentrations we expect Br_2^\perp to dominate.

Br_2^\perp represents a very unusual configuration for bromine. It shows strong charge transfer (0.129e) from the graphene, with a very strong induced molecular dipole ($\text{Br}^{+0.480}\text{-Br}^{-0.609}$). The singly occupied p_z -orbital of the lower Br atom depopulates into the p_z of the upper Br atom forming a nascent Bromonium and Bromide ion pair. In this way the emptied lower p_z -orbital can sit within the graphene π -cloud (Br only 2.74 \AA above the graphene).

This behaviour is reminiscent of the well-known reaction between Br_2 and unsaturated bonds in organic chemistry. However in these cases this dipolar form of Br_2 is an unstable transient state that immediately saturates the C=C bond, forming two Br-C bonds. In graphene this final step would be endothermic due to steric hindrance between the Br atoms as a result of the mechanical confinement of the lattice. Indeed our attempts to stabilise C-Br pairs on graphene in both neighbouring (1,2) and cross-hexagon (1,4) configurations both resulted in Br spontaneously reconstructing into a Br_2 molecule (placing Br-C in a (1,4) configuration with Br atoms on opposite sides of the graphene is 1.68eV less stable than Br_2^\perp).

The unusual Br_2^\perp configuration is reflected in the band structure (Figure 2a). The strong coupling between the graphene LUMO and the Br_2 antibonded state at around +0.6 eV reflects the interaction between the empty Br p_z -orbital and the graphene π -cloud, with the resultant low density Br_2 layer opening a small 86meV band gap.

In contrast Br_2^\parallel has no induced dipole, with weaker charge transfer (0.084e) from the graphene. The molecule sits 3.254 \AA above the graphene *i.e.* above the π -cloud, with the additional charge occupying the Br_2 $pp\sigma^*$ antibonding state. The band structure (Figure 2b) shows the Br_2 states lie lower than those of Br_2^\perp by $\sim 0.7\text{eV}$. The Br_2 anti-bonded state pins the Fermi level $\sim 0.2\text{eV}$ lower than in the pristine case, leaving graphene states around the K-point depopulated, indicating charge transfer from graphene to Br_2 . The Bromine states are flat and largely decoupled from the graphene bands since there is only weak interaction between Br_2 orbitals and the graphene π -cloud in this orientation.

Our results are consistent with experimental Raman observations of brominated graphene³. While for

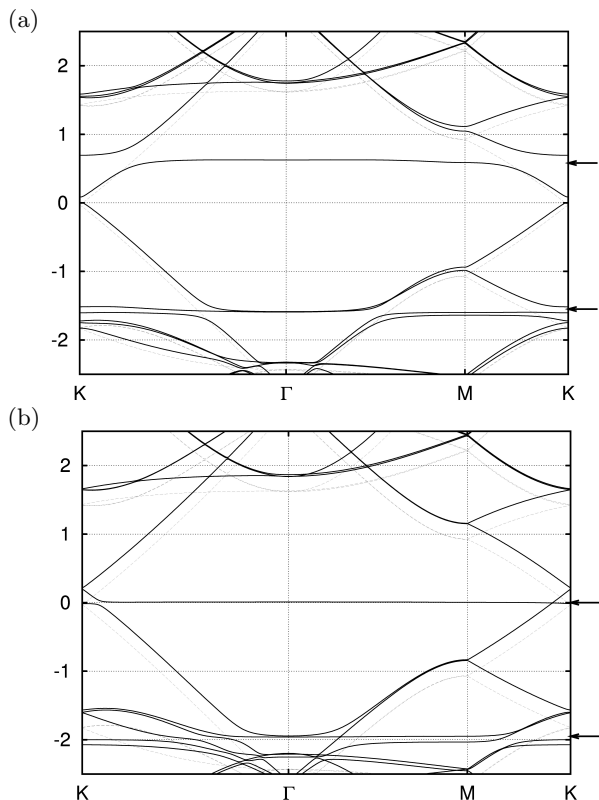


FIG. 2. Band structure of (a) Br_2^\perp and (b) Br_2^\parallel on graphene (eV), faded dotted lines indicate the same supercell of pristine graphene for comparison. Arrows indicate bromine related states.

graphene with three or more layers a resonant Raman signal was observed for Br_2 at around 240cm^{-1} , for mono- and bi-layer graphene no bromine signal was observed. This could be an orientation effect, since if the Br_2 sits perpendicular to the surface as we propose and orthogonal Raman is used, then the molecules will be aligned with the beam and there will be no interaction and hence no signal. In addition the bromine HOMO/LUMO states are further apart for Br_2^\perp ($\sim 2.2\text{eV}$) than for Br_2^\parallel (~ 1.96) or the various graphite structures we have examined (1.7-2.0eV). Given the excitation laser used (633nm, 1.96eV), Br_2^\perp may not be in resonance as the authors suggested³. Br_2^\parallel would have an associated Raman signal, and since none is observed this allows us to exclude this configuration. We note that the strong dipole of Br_2^\perp will make the molecule infra-red active.

We now turn our attention to graphite. Our calculated energy to separate AB graphite layers is 36.7 meV/atom, with AA stacked graphite 12.0meV/atom less stable than AB stacked graphite. These figures are in good agreement with experiment (35meV/atom²³) and previous calculations (9.68-9.70meV/atom AA/AB energy difference^{24,25}). Our interlayer spacings of 3.39Å and 3.50Å for AB and AA-stacked graphite respectively are also in reasonable agreement with previous

TABLE II. Calculated and experimental results for Br_2 intercalated graphite. The C-C layer distance refers to the layers separated by bromine. Experimental values from EXAFS¹⁰, Raman^{11,13} and XRD^{6,9,12,26}. At these low concentrations Br_2 intercalation is endothermic.

	Stage-1	Stage-2	Experiment	
Cell used	C_{18}Br_2	C_{72}Br_4		
Binding Energy/ Br_2 (eV)	+0.08	+0.08		
C-C layer distance (Å)	6.45	6.47	7.0 ^{9,12}	7.05 ²⁶
c-axis (Å)	9.80	9.82	10.7 ⁶	
Br-Br bond length (Å)	2.30	2.30	2.34 ^{10,27,12}	
Br-C distance (Å)	3.51	3.46	2.9 ¹⁰	
Br-Br frequency (cm^{-1})	287	274	242-258 ^{11,13}	
Charge transfer / Br_2 (e)	-0.10	-0.12	-0.16 ²⁷	-0.34 ¹³

calculations²⁵.

We placed Br_2 in a variety of different orientations and locations including above α - and β - carbon atom sites and hexagon centers, in graphite of various layer stackings. Unlike graphene, Br_2 in graphite is more stable parallel to the graphitic layers with Br atoms above hexagon centers (see Table II), in agreement with experiment^{6,10}. Perpendicular oriented Br_2 structures are much less stable (by typically 0.52eV). The results are summarised and compared with experiment in TableII. We note that the charge transfer value from Raman was reported with a large uncertainty¹³.

Besides the lowest energy structures quoted here we obtained many metastable structures. While their energies were all within 0.01-0.05eV of those structures discussed here, they show significant variation in the Br_2 stretch frequency (250-278 cm^{-1}), and slight variation in position and Br-Br bond length (2.31-2.33Å). This suggests that at room temperature Br_2 in graphite will be mobile, and is consistent with the observation of a broad and somewhat complicated Raman peak¹¹.

We explored all possible layer stacking combinations for stage-1 and stage-2 intercalated graphites. Bromine molecules are most stable with AA-stacked graphite each side, while unbrominated graphite layers preferentially are AB stacked. Thus (indicating layers of bromine molecules by X) we find the most stable stage-1 phase to be $[\text{AX}]_n$, and stage-2 to be $[\text{AXABXB}]_n$, suggesting $[\text{AXAB}]_n$ and $[\text{AXABABXBAB}]_n$ for stage-3 and stage-4 respectively.

Our calculated bromine intercalation energy is weakly endothermic, since at these low densities the energetic cost associated with separating graphite planes (a cost per unit area) is not sufficiently offset by the binding energy of Br_2 to the layers. Subtracting the energy to separate graphite layers from the Br_2 intercalation energy gives an energy for intercalation of Br_2 into 'pre-separated stage-1 graphite' of 0.581eV/ Br_2 . This implies that the *minimum* Br_2 concentration for exothermic intercalation in stage- n graphite will be $\text{C}_{16n}\text{Br}_2$. Indeed

a fixed-Br calculation for a C_8Br_2 stage-1 high coverage structure gives Br_2 intercalation as exothermic. Thus Br_2 will aggregate in the same inter-layer space and should be considered as a layer rather than individual molecules.

This minimum required concentration also suggests intercalation will be a slow diffusion process with an abrupt diffusion front. This is consistent with long experimental intercalation times²⁸, despite the high bromine inter-layer mobility. It also explains why, on out-gassing bromine, the material switches from a stage-2 to compound to stage- n ($n=3, 4, \dots$) rather than remaining stage-2 with lower bromine density per layer^{2,11,28}.

We note that frequency calculations incorporating the energetic double derivatives of surrounding carbon atoms gave identical values to within 1 cm^{-1} , showing that the Br_2 stretch mode is decoupled from the surrounding carbon lattice consistent with the literature¹.

Band structure calculations of Br_2 layers between graphite sheets (not shown here) give a bromine-related state which pins the Fermi level just below that of perfect graphite ($\sim 0.1\text{eV}$) indicating charge transfer from graphite to Br_2 . This state shows some dispersion indicating weak coupling with the underlying graphite. In other respects the graphite band structures are barely perturbed.

Our results on graphite and graphene can explain the anomalously large G peak shift for single graphene sheets in comparison with few-layer graphene³. Since the higher maximum Br_2 surface density for $Br_2^{\frac{1}{2}}$ than for inter-layer Br_2 means charge transfer per unit area will be higher. Additionally Br_2 can attach to both sides of graphene. We find a binding energy of $-0.38\text{eV}/Br_2$ for two $Br_2^{\frac{1}{2}}$ either side of the same C atom, with associated charge transfer of $-0.12e/Br_2$. Thus the net total charge transfer per unit area will indeed be significantly higher for monolayer graphene than multi-layer systems.

Test calculations for a (5,5) single walled nanotube, either isolated or in bundles, gave similar structural behaviour, *i.e.* Br_2 on the surface of the isolated tube adopts a perpendicular orientation, while intercalated Br_2 sits parallel to the tube walls. This will be explored further in a later publication.

In summary, we have examined low density Br_2 adsorption in graphene and graphite. On graphene Br_2 adopts an unusual perpendicular orientation, opening a small band gap ($\sim 86\text{meV}$) in the graphene with strong charge transfer. The molecule forms a $Br^+ + Br^-$ pair, rendering it infra-red active. This is a new form of Br_2 previously only considered as an unstable intermediate to bromine induced carbon bond saturation. Such graphene-induced stabilisation behaviour may be mirrored in other molecular species, enabling study of otherwise unstable reactive molecular forms.

In graphite Br_2 adopts a parallel orientation to the sheets with an associated charge transfer. Our calculations are in good agreement with experimental data where available. At high bromine concentrations and low temperatures there is some evidence of bromine chain structure formation^{29,30} in graphite, and we are currently investigating this further. We note that high density bromination of graphite leads to stage-2 compounds, and in conjunction with an appropriate secondary surfactant this may be a promising way to produce bilayer graphene.

ACKNOWLEDGMENTS

CPE and PW thank the “NANOSIM. GRAPHENE” project ANR-09-NANO-016-01 funded by the French National Agency (ANR) within the P3N2009 programme.

* Corresponding Author : chris.ewels@cncrs-immn.fr

¹ J. Seung-Hoon, S. G. Louie, and M. L. Cohen, Sol. Stat. Commun. **123**, 495 (2002).

² M. S. Dresselhaus and G. Dresselhaus, Advances in Physics **51**, 1 (2002).

³ N. Jung, N. Kim, S. Kockusch, N. J. Turro, P. Kim, and L. Brus, Nano Letters **9**, 4133 (2009).

⁴ S. Bandow, G. Chen, G. U. Sumanasekera, R. Gupta, M. Yudasaka, S. Iijima, and P. C. Eklund, Phys. Rev. B **66**, 075416 (2002).

⁵ T. Yoichi, Y. Yasuko, A. Noboru, and S. Yashushi, Ceramic Society of Japan **111**, 42 (2003).

⁶ W. T. Eeles and J. A. Turnbull, Proc. Roy. Soc. A **283**, 179 (1965).

⁷ B. Bach, M. Bagouin, F. Bloc, and A. Herold, C.R. Academic Science, Paris **257**, 681 (1963).

⁸ K. K. Bardhan, J. C. Wu, and D. D. L. Chung, Synth. Metals **2**, 109 (1980).

⁹ T. Sasa, Y. Takahashi, and T. Mukaibo, Carbon **9**, 407 (1971).

¹⁰ S. M. Heald and E. A. Stern, Phys. Rev. B **17**, 4069 (1978).

¹¹ P. C. Eklund, N. Kambe, G. Dresselhaus, and M. S. Dresselhaus, Phys. Rev. B **18**, 7069 (1978).

¹² A. Erbil, A. R. Kortan, R. J. Birgeneau, and M. S. Dresselhaus, Phys. Rev. B **28**, 6329 (1983).

¹³ A. Erbil, G. Dresselhaus, and M. S. Dresselhaus, Phys. Rev. B **25**, 5451 (1982).

¹⁴ D. Duan, Y. Liu, Y. Ma, Z. Liu, T. Cui, B. Liu, and G. Zou, Phys. Rev. B **76**, 104113 (2007).

¹⁵ J. E. Cahill and G. E. Leroi, Chem. Phys. **51**, 4514 (1966).

¹⁶ E. Widenkist, D. Boukhvalov, S. Rubino, S. Akhtar, J. Lu, R. A. Quinlan, M. I. Katsnelson, M. K. Leifer, H. Grennberg, and U. Jansson, J. Appl. Phys. D **42**, 112003 (2009).

¹⁷ A. N. Rudenko, F. J. Keil, M. I. Katsnelson, and A. I. Lichtenstein, Phys. Rev. B **82**, 035427 (2010).

¹⁸ P. R. Biddon and R. Jones, Phys. Stat. Solidi B **217**, 131 (2000).

¹⁹ I. Suarez-Martinez, A. A. El-Barbary, G. Savini, and M. I. Heggie, Phys. Rev. Lett. **98**, 015501 (2007).

- ²⁰ C. Hartwigsen, S. Goedecker, and J. Hutter, Phys. Rev. B **58**, 3641 (1998).
- ²¹ H. J. Monkhorst and J. D. Pack, Phys. Rev. B **13**, 5188 (1976).
- ²² M. S. Miao, V. E. Van Doren, and J. L. Martins, Phys. Rev. B **68**, 094106 (2003).
- ²³ L. X. Benedict, N. G. Chopra, M. L. Cohen, A. Zettl, S. G. Louie, and V. H. Crespi, Chem. Phys. Lett. **286**, 490 (1998).
- ²⁴ R. H. Telling and M. I. Heggie, Phil. Mag. Lett. **83**, 411 (2003).
- ²⁵ J. C. Charlier, X. Gonze, and J. P. Michenaud, Europhys. Lett. **208**, 403 (1994).
- ²⁶ W. Rudorff, Z. Anorg. Allg. Chem **245**, 383 (1941).
- ²⁷ S. M. Heald and E. A. Stern, Synth. Met. **1 (3)**, 249 (1980).
- ²⁸ J. E. Fischer, Acc. Chem. Res. **35**, 1079 (2002).
- ²⁹ D. D. L. Chung, Phase transitions **8**, 35 (1986).
- ³⁰ D. Chung, G. Dresselhaus, and M. S. Dresselhaus, Mat. Sci. Eng. **31**, 107 (1977).